Plasma temperatures in Saturn's ionosphere

Luke Moore,[1] Marina Galand,[2] Ingo Mueller-Wodarg,[2] Roger Yelle,[3] and Michael Mendillo[1]

[1] We have calculated self-consistent electron and ion temperatures in Saturn's ionosphere using a series of coupled fluid and kinetic models developed to help interpret Cassini observations and to examine the energy budget of Saturn's upper atmosphere. Electron temperatures in the midlatitude topside ionosphere during solar maximum are calculated to range between 500 and 560 K during the Saturn day, approximately 80–140 K above the neutral temperature. Ion temperatures, calculated for only the major ions H^+ and H_3^+, are nearly equal to the neutral temperature at altitudes near and below the height of peak electron density, while they can reach 500 K during the day at the topside. Plasma scale heights of the dusk electron density profile from radio occultation measurements of the Voyager 2 flyby of Saturn have been used to estimate plasma temperature as a comparison. Such an estimate agrees well with the temperatures calculated here, although there is a topside enhancement in electron density that remains unexplained by ionospheric calculations that include photochemistry and plasma diffusion. Finally, parameterizations of the heating rate from photoelectrons and secondary electrons to thermal, ambient electrons have been developed. They may apply for other conditions at Saturn and possibly at other giant planets and exoplanets as well.

Citation: Moore, L., M. Galand, I. Mueller-Wodarg, R. Yelle, and M. Mendillo (2008), Plasma temperatures in Saturn's ionosphere, *J. Geophys. Res.*, *113*, A10306, doi:10.1029/2008JA013373.

1. Introduction

[2] Determination of the plasma temperature within an ionosphere is an important and complicated task. Electron and ion temperatures can vary significantly above the ambient neutral temperature over the course of a planetary day, affecting the outcome of many ionospheric phenomena, from the most basic (e.g., chemical reaction rates) to the more complex (e.g., plasma diffusion), and they play an important role in the coupling between an ionosphere and magnetosphere [*Nagy et al.*, 1986].

[3] It was not until the early 1960s that it became obvious that electron temperatures were sometimes much larger than neutral temperatures in the terrestrial ionosphere, particularly at altitudes near and above the F region [*Bourdeau*, 1963]. Since that time, dramatic advances have been made in understanding the physical theory and measuring the parameters relevant to plasma temperature calculations, as summarized by, for example, *Banks and Kockarts* [1973], *Cicerone et al.* [1973], and *Schunk and Nagy* [2008].

[4] Where observations of plasma temperature are not available (e.g., there has never been an in situ observation within the ionosphere of a giant planet), modeling must play a central role in order to thoroughly understand an ionosphere. At Earth, nearly a century of aeronomic studies has resulted in three-dimensional general circulation models (GCMs) that can calculate, among many other properties, ion and electron temperatures throughout the terrestrial ionosphere from first principles [*Roble and Ridley*, 1994; *Fuller-Rowell et al.*, 1996]. These calculations have been shown to reproduce observed temperatures [*Lei et al.*, 2007]. The basic theory applies equally well in other planetary ionospheres, although it is not as fully developed, mostly owing to the paucity of observations required to constrain atmospheric parameters and planet-specific reaction rates and cross sections.

[5] This paper presents plasma temperature calculations for Saturn based on the recently developed Saturn Thermosphere-Ionosphere-Model (STIM), a Saturn GCM, and an associated group of 1-D submodels developed in preparation for the Cassini era [*Moore et al.*, 2004; *Mueller-Wodarg et al.*, 2006]. Section 2 introduces briefly the relatively few past plasma temperature studies performed at Jupiter and Saturn, while section 3 (and Appendices A and B) provides the framework for the new calculations introduced here. Finally, results are presented and discussed in section 4.

2. Background: Plasma Temperatures at Jupiter and Saturn

[6] Plasma temperatures in the Jovian ionosphere were first calculated on the basis of the assumption of local energy balance [*Henry and McElroy*, 1969; *Prasad and*

---

[1]Center for Space Physics, Boston University, Boston, Massachusetts, USA.
[2]Space and Atmospheric Physics Group, Department of Physics, Imperial College London, London, UK.
[3]Lunar and Planetary Laboratory, University of Arizona, Tucson, Arizona, USA.

Capone, 1971], resulting in thermal equilibrium between ions, electrons, and neutrals at altitudes where $[H_2] > \sim 5 \times 10^8 \, cm^{-3}$. This conclusion followed from two factors: (1) the efficient electron energy sink provided by rotational and vibrational excitation of H_2 and (2) the strong coupling between ions and neutrals due to symmetrical resonance charge exchange between H^+ and H [*Henry and McElroy*, 1969]. *Nagy et al.* [1976] and *Goertz* [1973] were among the first to include heat conduction in their electron temperature calculations as well as examine the effect of plasmaspheric heat inflow. They found that a heat influx of $\sim 10^8 \, eV \, cm^{-2} \, s^{-1}$ was sufficient to raise the electron temperature substantially above the neutral temperature in the low neutral density region ($<10^9 \, cm^{-3}$) above the ionospheric peak [*Nagy et al.*, 1976; see also *Swartz et al.*, 1975]. More recently, IR observations of emission from H_3^+ have revealed ion temperatures between ~ 700 and 1250 K, even in nonauroral regions [see *Miller et al.*, 2000, and references therein], presenting some difficulty for theoretical models [e.g., *Achilleos et al.*, 1998].

[7] Plasma temperature calculations at Saturn draw heritage from terrestrial and Jovian studies. To date, there are only two theoretical determinations of ion and electron temperatures in Saturn's ionosphere [*Waite*, 1981; *Glocer et al.*, 2007]. *Waite* [1981] predicted ion and electron temperatures ranging from 1000 K to 100,000 K, depending on the values of various assumed parameters, such as ion-neutral differential velocities (leading to joule heating) and downward heat fluxes at the upper boundary. However, those calculations were performed using a neutral temperature profile with an exospheric temperature of ~ 1000 K (compared with the 420 K later derived from Voyager measurements [*Smith et al.*, 1983]). Since the Voyager observations indicated that the model's assumed exospheric temperature was too high, a new derivation based on more recent spacecraft data and laboratory rates was warranted. *Glocer et al.* [2007] addressed the high-latitude ionosphere, using a 1-D multifluid model to study the polar wind at Saturn. Using a magnetospheric topside heat flux of $\sim 10^{10} \, eV \, cm^2 \, s^{-1}$ (A. Glocer, personal communication, 2008), *Glocer et al.* [2007] derived peak ion temperatures between 1500 and 3000 K, depending on the assumed background atmosphere.

[8] On the basis of the assumption of an isothermal upper atmosphere, plasma temperatures at Saturn have been estimated from Pioneer and Voyager electron density scale heights to range between ~ 600 and 1700 K [*Atreya et al.*, 1984; *Moore and Mendillo*, 2005]. There are, however, a number of problems with estimating plasma temperatures from electron density scale heights, $H_p = \frac{2kT_p}{m_i g}$ (where $T_p = 1/2(T_i + T_e)$ is the plasma temperature). Most notably, the assumed ion mass (determined by ion composition) m_i is an important factor in the final estimate, and small altitude gradients in temperature can lead to ambiguous results. In addition, the giant planets have global magnetic fields, and thus it is not possible to estimate plasma temperatures from scale heights in equatorial regions where the magnetic field is perpendicular to the zenith and therefore inhibits plasma motions in that direction.

3. Modeling Approach

[9] The neutral atmosphere used in this study comes from the Saturn Thermosphere-Ionosphere-Model (STIM), a 3-D general circulation model of Saturn's upper atmosphere [*Mueller-Wodarg et al.*, 2006]. STIM solves globally the coupled nonlinear Navier-Stokes equations of energy, momentum and continuity for Saturn's major neutral species by explicit time integration (a numerical filter is used to damp the growth of fluctuations in the solution at wavelengths smaller than the grid resolution). Hydrostatic equilibrium is assumed in the local vertical direction. The energy input considered in this study is of solar origin and is specified using the EUVAC model, an empirical model of solar soft X-ray and EUV radiation [*Richards et al.*, 1994].

[10] In order to calculate ion and electron temperatures, a self-consistent determination of the heating rates of the ambient, thermal electrons by the suprathermal electrons (e.g., primary photoelectrons, secondary electrons) is required, which is a computationally intensive task for a GCM. Rather than parameterize this complex interaction without detailed calculations to verify the accuracy of the parameterization, we preferred to utilize a separate one-dimensional suprathermal electron transport model, described below.

[11] Assuming there is no applied electric field and that charged particle motions are constrained by the planetary magnetic field, the thermal ion and electron energy equation can be written [*Banks*, 1967; *Chapman and Cowling*, 1970]

$$\frac{\partial T}{\partial t} + v \sin^2 I \frac{\partial T}{\partial z} + \frac{2}{3} T \sin^2 I \frac{\partial v}{\partial z} - \frac{2}{3} \frac{\sin^2 I}{nk} \frac{\partial}{\partial z} \left(\Gamma \frac{\partial T}{\partial z} \right)$$
$$= \frac{2}{3} \frac{1}{nk} [Q - L] \tag{1}$$

where T is ion or electron temperature, I is magnetic dip angle, v is vertical drift, n is ion or electron density, k is Boltzmann's constant, Γ is thermal conductivity, Q is heating rate, L is cooling rate, and t and z represent time and altitude, respectively. The primary difficulty in calculating ion and electron temperatures, then, lies in determining accurate heating Q and cooling L terms for each time step.

[12] The basic cause of thermal disequilibrium in an ionosphere is that ionizing photons or energetic charged particles generally possess more energy than the ionization threshold of neutrals, meaning the freed electrons will carry most of that excess away as kinetic energy [e.g., *Rishbeth and Garriott*, 1969; *Schunk and Nagy*, 2008]. Primary photoelectrons and secondary electrons then lose their energy via a series of collisions with the ambient electron, ion and neutral gases. In denser regions of the atmosphere (i.e., at lower altitudes), collisions with the neutrals are frequent enough that the energetic photoelectrons thermalize before they can recombine, and neutral densities are large enough that the neutral temperature remains unchanged. At altitudes near and above the electron density peak, photoelectrons are efficient at heating the ambient electron population via long-range Coulomb collisions. As photoelectrons and their secondaries are the dominant source of heating for the thermal electrons, and an important ionization source, it is necessary to describe the transport and degradation of energetic electrons throughout the atmosphere in order to accurately model the properties of an ionosphere. In practice, this is a complex problem that requires knowledge of atomic and molecular structure,

electron impact cross sections, scattering functions, and ionospheric plasma temperatures and densities.

[13] Three approaches to describe the transport of photoelectrons in the terrestrial ionosphere were explored initially: (1) diffusion equation formulation [*Nisbet*, 1968], (2) two-stream approximation of the Boltzmann equation [e.g., *Nagy and Banks*, 1970; *Stamnes and Rees*, 1983; *Richards and Khazanov*, 1997], and (3) tracking the paths of individual particles using a Monte Carlo method [*Cicerone and Bowhill*, 1971]. *Cicerone et al.* [1973] analyzed the inherent strengths and weaknesses of these three approaches in detail. More recently, a multistream approach for solving the Boltzmann equation has been applied to the transport of photoelectrons [*Strickland et al.*, 1976; *Lilensten et al.*, 1989; *Lummerzheim and Lilensten*, 1994; *Nilsson et al.*, 1996], which is the method used here. Our multistream transport model applied to suprathermal electrons is based on the solution proposed by *Lummerzheim et al.* [1989] for terrestrial applications and validations [*Lummerzheim and Lilensten*, 1994]. It has been adapted to Titan's ionosphere [*Galand et al.*, 1999, 2006] and is adapted here to Saturn's ionosphere.

[14] In order to derive self-consistent ion and electron temperature calculations we couple three codes sequentially. The codes used are (1) a 1-D version of the STIM thermosphere, described below, (2) the 1-D ionospheric module, and (3) the electron transport code. All of the 1-D modules discussed here are essentially 2-D, as they solve in altitude via explicit time integration, thereby allowing diurnal variations to result from the changing solar zenith angle. The coalignment of Saturn's rotational and magnetic axes along with the lack of topographical features means that local time is basically equivalent to longitude at Saturn. Magnetic dip angles are calculated using an aligned dipole. Preliminary results using the Saturn Pioneer Voyager model [*Davis and Smith*, 1990], a more accurate description of Saturn's magnetic field, indicate no substantial deviations from the results presented below.

[15] The STIM GCM provides the neutral background parameters: density, wind, and temperature structure. In this case, we used a one-dimensional version of STIM rather than the full 3-D GCM, as suprathermal electron transport calculations require a grid with much higher altitude resolution ($5-25$ km) and a lower altitude boundary (590 km) than the standard 3-D GCM can provide within a reasonable time frame. The neutral atmosphere extends from 5×10^{-3} mbar (around 590 km above the 1 bar level) to around 10^{-11} mbar and contains the principal gases H, H_2 and He as well as CH_4. A diffusive equilibrium distribution is assumed, which was calculated with a 1-D diffusion model derived from the 3-D GCM, using an eddy diffusion coefficient identical to that of *Moses et al.* [2000], placing the CH_4 homopause near the 1.7×10^{-5} mbar level. The CH_4 mixing ratios are a good fit to observations as reviewed by *Moses et al.* [2000]. We assume a thermal profile consistent with observations by *Smith et al.* [1983] and *Hubbard et al.* [1997], with exospheric temperatures (above the 2×10^{-7} mbar level) of 420 K and temperatures in the mesosphere (below the 10^{-4} mbar level) constant at 136 K. This thermosphere remains as a constant background throughout the rest of the calculations.

[16] On the basis of the STIM neutral background, the one-dimensional ionospheric module computes ion and electron density profiles at a specific latitude as a function of local time, assuming thermal equilibrium among electrons, ions, and neutrals. The STIM 1-D ionospheric module solves the equations of ion continuity and momentum using the methods and rates described by *Moore et al.* [2004]. Next, the suprathermal electron transport code applied to photoelectrons and secondary electrons acts upon this ionosphere. This results in estimates of the heating rates of the ambient, thermal electrons for each of the 24 hours of Saturn local time (i.e., $24 \sim 27$ min intervals comprising the full ~ 10.7 hour Saturn day). Ion and electron temperatures are then recomputed within the ionospheric module, along with new ion and electron density profiles, as plasma chemistry and diffusion are perturbed by the nonequilibrium temperatures from the energy transport routine. Finally, this coupling process between the ionospheric module and the transport code is repeated until convergence is reached. A more detailed description of the photoelectron transport code is given in Appendix A, along with the explicit formulae and parameters used to solve the ion and electron energy equations (Appendix B).

[17] Another important calculation that is made using the above codes is to quantify the effect of secondary ionization at Saturn. This will be the focus of a separate study (M. Galand et al., Modeling the photoelectron secondary ionization process at Saturn, submitted to *Journal of Geophysical Research*, 2008). Model results presented here include the effects of secondary electrons as this population is produced dominantly at heights where it has a relatively small effect upon thermal balance. For example, while secondary ionization in Saturn's ionosphere can lead to an enhancement in the peak electron density of $\sim 30\%$, its maximum effect on peak electron temperatures is only to reduce the peak electron temperature by $\sim 4\%$.

4. Results

[18] We chose to model the Voyager 2 ionospheric conditions [*Tyler et al.*, 1982; *Lindal et al.*, 1985]. This period is beneficial to a pilot plasma temperature study in a number of ways: there is a radio occultation $N_e(h)$ measurement at midlatitude (i.e., $\sim 30°N$), describing a relatively smooth electron density profile (by outer planet standards), and there is a contemporaneous measurement of the exospheric temperature to constrain the background atmosphere [*Smith et al.*, 1983]. Plasma temperatures at midlatitudes might be considered "first-order" solutions to the global electron and ion temperatures in that they are relatively isolated from the complications of processes specific to the equatorial or polar ionospheres, such as vertical electrodynamics, magnetospheric electric fields, joule heating and particle precipitation. The Voyager 2 duskside ionosphere profile is not entirely smooth, however its systematic decline above the electron density peak is likely indicative of average conditions at Saturn, precluding the necessity of modeling the sharp ionospheric layers frequently observed [*Nagy et al.*, 2006] whose origin is poorly understood [e.g., *Moses and Bass*, 2000; *Moore and Mendillo*, 2007]. While it would be more current to model the Cassini era conditions, the electron density profiles available at present do not share
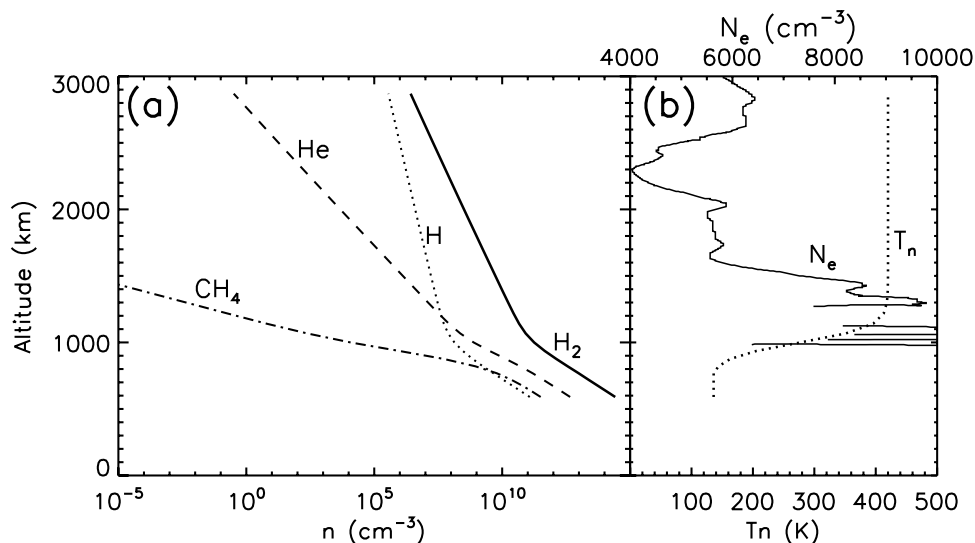
Figure 1. STIM neutral atmospheric (a) density and (b) temperature altitude profiles at local noon for Voyager 2 flyby conditions: 30°N latitude with a solar declination of +2.7° (solar zenith angle of 87°) and an F10.7 of 267. The exospheric temperature of 420 K [*Smith et al.*, 1983] is reproduced using a combination of wave and joule heating, as described by *Mueller-Wodarg et al.* [2006]. The range of modeled pressure levels is $0.5-7.4 \times 10^{-9}$ mbar. Also shown in Figure 1b is the ingress electron density profile measured at Saturn dusk by Voyager 2 [*Tyler et al.*, 1982]. The highly structured ionospheric layers at 1000 km reach nearly 10^5 e^- cm^{-3}, but at altitudes where large neutral densities lead to thermal equilibrium ($T_e = T_i = T_n$).

any of the benefits mentioned above. Specifically, the 12 Cassini profiles are all equatorial and highly structured [*Nagy et al.*, 2006]. Moreover, there are no measurements yet available to constrain the background thermosphere during the Cassini era.

[19] The neutral atmosphere produced by STIM for the Voyager 2 flyby on 26 August 1981 is presented in Figure 1 together with the Voyager 2 ingress electron density profile. On this day, Saturn was near its equinox, with a solar declination of +2.7°, and the solar cycle was near its maximum, with an F10.7 of 267. Solar heating alone does not provide enough energy to heat Saturn's thermosphere to the observed values (a common problem for all the giant planets [e.g., *Yelle and Miller*, 2004]), and so in order to reproduce the observed exospheric temperature of 420 K [*Smith et al.*, 1983], STIM employs a combination of wave and joule heating, as described by *Mueller-Wodarg et al.* [2006].

[20] Despite considerable structuring, the Voyager 2 dusk electron density profile is quite smooth in comparison to other Pioneer, Voyager and Cassini profiles [*Atreya et al.*, 1984; *Nagy et al.*, 2006]. Its maximum electron density, of nearly 10^4 e^- cm^{-3}, occurs at ~1300 km altitude, with a relatively steady decline above the peak interrupted by an extended enhancement in electron density at the topside. This topside "bulge" is likely due to some unknown transport effect, and could not be caused by plasma diffusion. Highly structured layers of electron density below the main peak extend to nearly 10^5 e^- cm^{-3} within a range of less than 100 km, and may be the result of gravity waves or other structures in the neutral winds [*Matcheva and Strobel*, 1999; *Moses and Bass*, 2000]. These layers occur in a very dense neutral atmosphere where thermal equilibrium ($T_e = $

$T_i = T_n$) holds and are not of crucial importance to this study for that reason. Therefore, for the remainder of the text, we focus on the nearly monotonically decreasing electron density profile between the peak and the topside "bulge," i.e., ~1300−2300 km.

4.1. Ionospheric Electron Heating Rates and Plasma Temperatures Under Sunlit Conditions

[21] As discussed in section 3, the suprathermal electron transport code acts upon Saturn's upper atmosphere in order to derive thermal electron heating rates as a function of altitude and local time. The resulting heating rates for three local times are shown in Figure 2. Peak heating rates vary by approximately a factor of five over the course of a Saturn day; at night, as there is no photoionization, there is consequently no thermal electron heating due to photo-electrons. These facts imply that diurnal variations in electron density will play an important role in determining the calculated electron and ion temperatures.

[22] Electron and ion temperatures calculated using the thermosphere presented in Figure 1 and the thermal electron heating rates of Figure 2 are shown in Figure 3. As before, this plot presents results for conditions of the Voyager 2 flyby. Contours of electron temperature, showing variations in altitude and local time, illustrate the diurnal behavior described above. Specifically, during the majority of night-time hours (~2100 LT to ~0600 LT), fast thermal quenching and the absence of a heat source lead to thermal equilibrium throughout Saturn's ionosphere. At altitudes below ~1000 km thermal equilibrium between the plasma and the neutrals persists throughout the Saturn day, as the higher neutral densities at low altitude lead to more frequent collisions, and thus increased quenching.
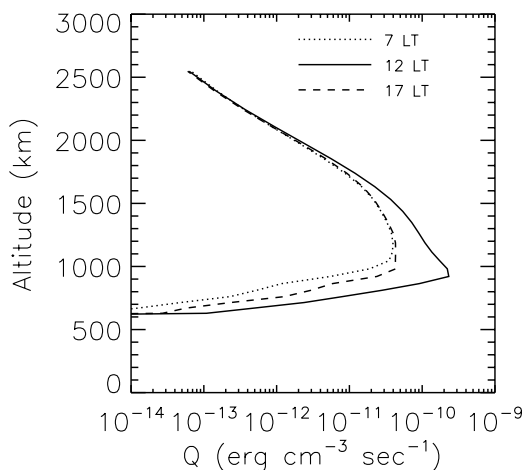
Figure 2. Altitude profiles of the thermal electron heating rates for Voyager 2 conditions at 30°N latitude for three local times on Saturn: 0700 LT, 1200 LT, and 1700 LT. The heating rates are calculated with a Saturn local time resolution of 1 hour using a comprehensive suprathermal electron transport model applied to photoelectrons.

[23] At sunrise, Saturn's ionosphere experiences a rapid heating. As evidenced in Figure 2, the dawn thermal electron heating rate profile is essentially equal to that at noon at altitudes above the electron density peak. The lowest electron densities of the Saturn day also occur just before dawn in the model (see Figure 4), meaning that the sudden introduction of a heating function upon a relatively tenuous ambient electron gas is a prime condition for efficient heating. Maximum ion and electron temperatures are reached shortly after sunrise, by ∼0800 LT. Plasma temperatures do not vary significantly from that maximum for the remainder of the Saturn day, despite an increasing heating function, as more frequent Coulomb collisions from an increasing electron density (Figure 4) remove more energy from the electron gas, and heat is transported vertically away. After sunset, these losses, along with plasma-neutral interactions, quench the electron and ion gases within three Saturn hours (∼80 min).

4.2. Ion and Electron Densities

[24] Model results for the diurnal variation of electron density during the Voyager 2 flyby conditions at Saturn are presented in Figure 4, along with electron and ion density altitude profiles at three selected local times. Thus, Figures 1–4 comprise a self-consistent set of STIM results for the Voyager 2 flyby. Ionospheric calculations include a nominal influx of neutral water (5 × 10⁶ H_2O molecules cm^{-2} s^{-1}), likely from Saturn's rings or icy moons (such as Enceladus [e.g., *Porco et al.*, 2006; *Waite et al.*, 2006]), which falls through the thermosphere in a matter of hours, charge-exchanging with protons along the way, thereby creating molecular ions that quickly recombine and reduce the net modeled electron density [*Moore et al.*, 2006]. Below ∼1000 km altitude, the electron density profile is dominated by hydrocarbon ions, whose formation represents a sink for the major ions reacting with methane in this study [*Moore et al.*, 2004]. For a full discussion of the

wealth of hydrocarbon ions in Saturn's lower ionosphere, see *Moses and Bass* [2000].

[25] One added benefit of knowing the ion and electron densities that correspond with the calculated plasma temperatures of Figure 3 is that it is possible to test the most common method of estimating plasma temperatures remotely, which involves making a series of assumptions regarding the topside plasma scale heights of radio occultations. It is standard to assume that the plasma temperature is isothermal; however, if even a small temperature gradient is present, it can introduce significant uncertainty in the final temperature estimate [*Nagy et al.*, 2006]. For the hydrogen-dominated atmospheres of the giant planets, it is reasonable to predict H^+ as the major topside ion. The model results presented in Figures 3 and 4 support these standard assumptions [see also *Majeed and McConnell*, 1991; *Moses and Bass*, 2000; *Moore et al.*, 2004]. Therefore, the model ionosphere presented here is one well suited to estimating plasma temperature from the topside plasma scale height. The model's dusk electron density scale height in Figure 4 is ∼750 km, which would lead to an estimated plasma temperature of ∼535 K, a value to be compared with the 480 K obtained from electron temperature calculations (Figure 3). This result demonstrates self-consistency in electron temperature between the explicit calculation and the estimation derived from the electron density in the midlatitude topside ionosphere, and therefore gives some measure of confidence that such estimations from radio occultation measurements are reasonable at Saturn.

4.3. Comparisons Between Model and Observations

[26] Part of the argument for including plasma temperature calculations within an ionospheric model is that thermal disequilibrium changes chemical reaction and ion diffusion rates, affecting modeled plasma densities. Thus, it is useful to compare our new results with ion and electron densities derived assuming thermal equilibrium. Such a comparison is shown in Figure 5, which plots two modeled electron density profiles (with and without temperature calculations) along with an observed profile. The Voyager 2 profile plotted here comes from radio occultation measurements made by Voyager 2 during its 26 August 1981 flyby of Saturn [*Tyler et al.*, 1982; *Lindal et al.*, 1985]. Two points are immediately clear from Figure 5: (1) the electron densities do not change dramatically in Saturn's ionosphere when ion and electron temperatures exceed the neutral temperature, and (2) there is an electron density enhancement present in the topside of the Voyager 2 profile not reproduced in the model. The modeled dusk electron density profile, consisting of predominantly H^+ and H_3^+ ions, is within 10% of the observed electron density peak of ∼9500 e^- cm^{-3} at 1300 km altitude. However, the modeled ionosphere is not able to capture the pronounced bulge of electron density observed by Voyager 2 at the topside (i.e., >2500 km).

[27] Also identified in Figure 5 are two representative plasma scale heights, H_{P1} and H_{P2}, which illustrate the range of positive plasma scale heights one might derive from the Voyager observation. H_{P1} represents a minimum in topside plasma scale height, and is derived from the Voyager 2 electron density profile between 2000 and 2300 km. H_{P2}, then, might be considered to be the maxi-
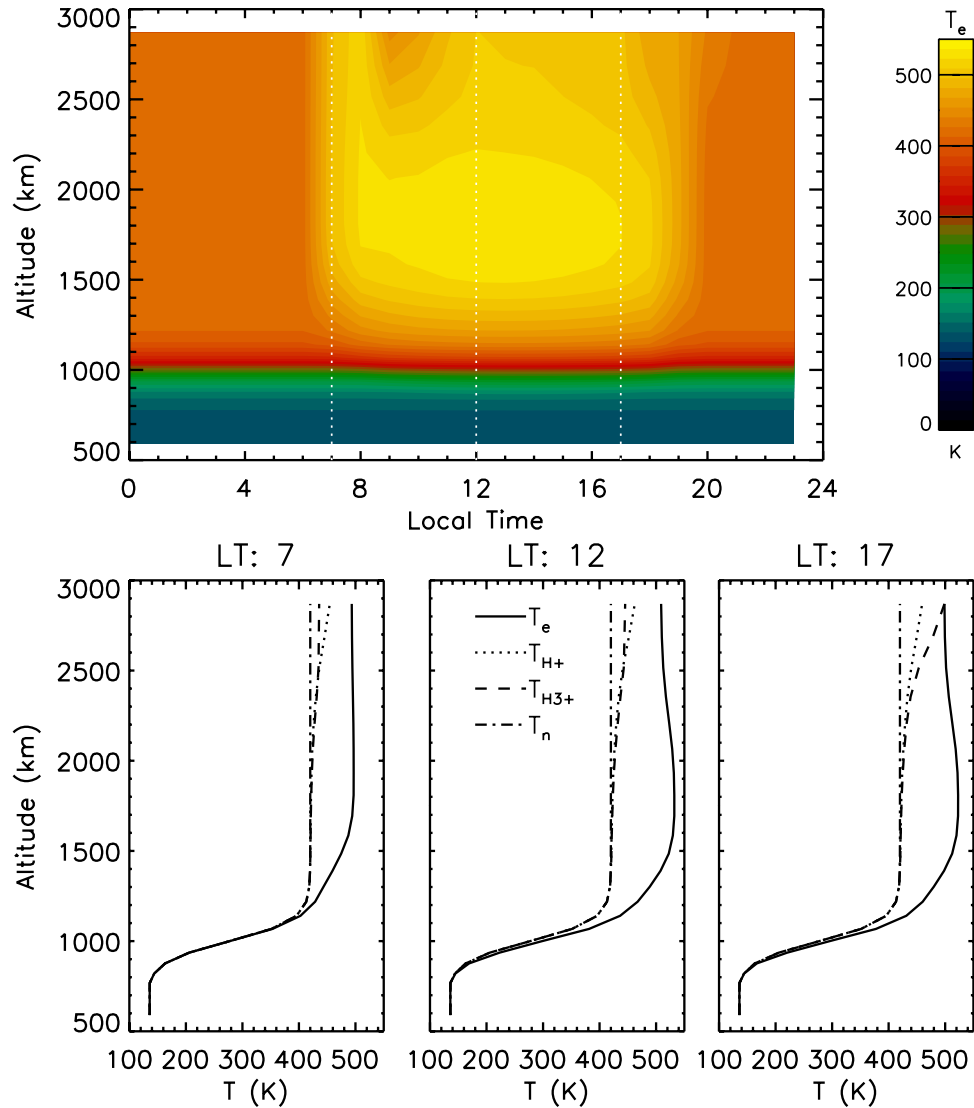
Figure 3. Model results. (top) Diurnal variation of electron temperature as a function of altitude and local time for Voyager 2 conditions at 30°N latitude using the heating rates of Figure 2. (bottom) Temperature altitude profiles, illustrating T_e (solid), T_{H^+} (dotted), T_{H3+} (dash), and T_n (dot-dash), are shown for 0700 LT Saturn time (left), 1200 LT Saturn time (middle), and 1700 LT Saturn time (right).

mum plasma scale height for the Voyager profile; it is defined in the 1300–2300 km altitude range, which represents the monotonic decline from the observed electron density peak to the pre-enhancement topside. The scale heights and inferred plasma temperatures for H_{P1} and H_{P2} are approximately 1050 km and 511 km, and 750 K and 370 K, respectively. Therefore, the 480 K temperature derived in the model is encompassed by the range of plasma temperatures estimated from the Voyager observation.

[28] The fact that calculated electron densities do not change dramatically when nonequilibrium plasma temperatures are included in the model means that (even if the model had under predicted temperatures in Saturn's ionosphere) it is not able to reproduce an electron density enhancement with a negative plasma scale height similar to that observed in the Voyager 2 profile with the processes discussed above. In other words, transport processes other than vertical plasma diffusion are likely the cause of such a topside enhancement in electron density. Preliminary calculations using a cool relaxed thermosphere, with $T_{exo} = 300$ K (compared with the 420 K thermosphere derived from Voyager observations [*Smith et al.*, 1983]), support this statement; they predict a plasma temperature of over 700 K, more than double the neutral temperature, yet the topside electron density is still well short of the observed Voyager enhancement. An examination of the relevant chemical reaction rates and vertical plasma fluxes helps to explain this discrepancy. At Saturn, the only important chemical reactions that are plasma temperature dependent are dissociative recombination rates, and those are inversely proportional to T_e to some fractional power [*Moses and Bass*, 2000]. Figure 6 presents the vertical diffusive fluxes of H^+ calculated within the model, from which it can be seen that because of the mostly isothermal electron temperature profile the temperature gradient term contributes very little to the net flux.
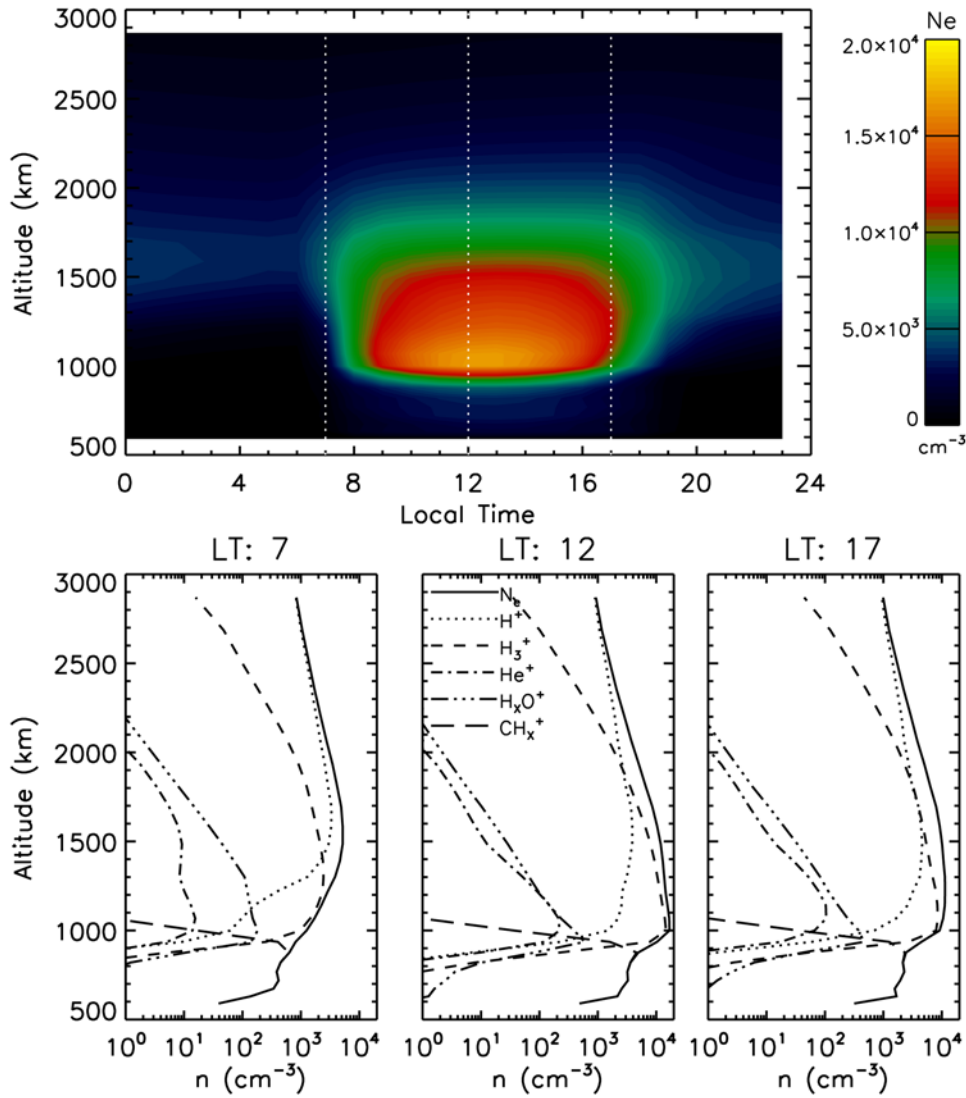
Figure 4. Model results. (top) Diurnal variation of electron density as a function of altitude and local time for Voyager 2 conditions at 30°N latitude. (bottom) Plasma density altitude profiles, illustrating H^+ (dotted), H_3^+ (dash), He^+ (dot-dash), $H_2O^+ + H_3O^+$ (i.e., water ions; dash-dot-dot-dot), CH_X^+ (i.e., hydrocarbon ions; long dash), and N_e (solid), are shown for 0700 LT Saturn time (left), 1200 LT Saturn time (middle), and 1700 LT Saturn time (right).

4.4. Parameterization of the Thermal Electron Heating Rate Due to Photoelectrons and Secondaries

[29] As full photoelectron transport calculations are not always viable, it is beneficial to also compute plasma temperatures in Saturn's ionosphere on the basis of parameterizations of the thermal electron heating rates. Deriving an accurate yet simplistic parameterization that yields nearly identical results to the full calculations allows for more comprehensive models, such as STIM, to include plasma calculations globally without requiring the addition of debilitating electron transport computations. Such an approach is already used in terrestrial GCMs, which incorporate parameterizations of the thermal electron heating rates associated with photoelectrons [e.g., *Roble et al.*, 1987; *Millward et al.*, 1996].

[30] The incident photoionization rate can quickly and easily be derived from the Beer-Lambert law, and therefore

it makes sense to use the photoionization profile in the parameterization. Figure 7 presents the diurnal variations of the ratio of two different parameterizations, described below, over the thermal electron heating rate derived from the full 1-D suprathermal electron transport code. In addition, the noontime electron temperature profile resulting from application of each of the three heating rates is given in Figures 7b and 7d.

[31] The simplest conversion between photoionization rates P and thermal electron heating rates induced by photoelectrons and secondaries Q_e is to multiply the calculated photoionization rates by some efficiency factor [e.g., *Swartz and Nisbet*, 1972], as the shapes of their profiles are generally similar. Figures 7a and 7b represent this scenario, where the photoionization rate for H_2^+ in ions cm^{-3} s^{-1} is used (i.e., the ion with the highest rate of photoproduction in Saturn's ionosphere [*Moore et al.*, 2004]). Calculations
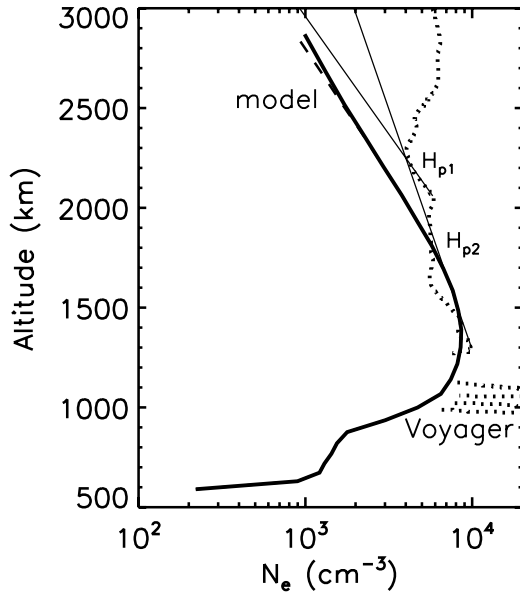
Figure 5. Comparison between modeled electron density calculations at 1800 LT that do (thick solid) and do not (dashed) include plasma temperature calculations. Note that minor differences occur only above 2300 km. In addition, the dotted curve shows the Voyager 2 ingress (dusk) radio occultation profile. Two slopes are plotted over the Voyager observation, H_{P1} and H_{P2} (thin solid lines), which describe a range of positive plasma scale heights estimated from the Voyager electron density profile (see text).

using $Q = (9 \times 10^{-12} \text{ erg}) P$ rather than the Q derived from the suprathermal electron transport calculations predict nearly the same topside plasma temperature (475 K), but are not able to reproduce the entire electron temperature structure, with deviations as large as 30 K at noon and up to 60 K at other local times. Figures 7c and 7d represent a more refined parameterization, which includes the noontime electron density profile as an additional free parameter:

$$Q(z,t) = \left(10^{-12}\text{erg}\right)c(z)P(z,t)\left[1 + \frac{N_{e,noon}(z)}{10^3\text{cm}^{-3}}\right], \quad (2)$$

where c is a parameterization constant whose value varies with altitude,

$$c = \begin{cases} 1.0 & z \leq 1800 \text{ km} \\ 1.2 & 1800 \text{ km} < z \leq 2300 \text{ km} \\ 1.5 & 2300 \text{ km} < z \leq 2600 \text{ km} \\ 2.25 & z > 2600 \text{ km} \end{cases} \quad (3)$$

The equivalent pressure ranges for c (corresponding to 1800 km, 2300 km, and 2600 km) are approximately 5.3×10^{-6} mbar, 3.4×10^{-7} mbar, and 6.5×10^{-8} mbar. This parameterization predicts electron temperatures within 9 K of the values derived from the full calculation at noon and never differs by more than 30 K at other local times. For both parameterizations, ion temperatures are always within 5 K of the full-calculation values. While these parameterized heating rates compare well with the suprathermal electron transport calculations for the specific conditions

at Saturn evaluated here (i.e., 2.7° solar declination, 30°N latitude, solar maximum), their reasonable agreement over a wide range of solar zenith angles implies that they might work equally well for other geometrical combinations at Saturn, and possibly in other hydrogen-rich atmospheres (e.g., Jupiter, exoplanets).

5. Conclusions

[32] Using a series of coupled models developed to help interpret Cassini observations and to study the energy budget in Saturn's upper atmosphere, we have calculated self-consistent electron and ion temperatures. The sole source of ionospheric heating evaluated here is due to photoelectrons and associated secondary electrons; consequently, combined with fast quenching, the model predicts thermal equilibrium ($T_e = T_i = T_n$) to be present throughout Saturn's ionosphere for most of the nighttime hours and for the full day at altitudes below ~1100 km. At sunrise, rapid heating of the ambient electron gas occurs; the rate of change in plasma temperature during subsequent daylight hours is lower than at sunrise, as electron and ion gas densities increase along with their temperatures.

[33] Our estimated electron temperatures in the topside ionosphere range between 500 and 560 K during the Saturn day, roughly 100 K above the neutral temperature. Ion temperatures, calculated for only the major ions H^+ and H_3^+, are nearly equal to the neutral temperature at most altitudes, while they can reach 500 K during the day at the topside. These relatively cool plasma temperatures do not affect the calculated ion and electron density profiles significantly. Therefore, enhancements observed frequently in topside electron density profiles retrieved from radio occultation measurements [*Atreya et al.*, 1984; *Nagy et al.*, 2006] are likely due to some other transport process, such as horizontal advection or plasma instabilities.

[34] Parameterizations of the thermal electron heating rate based on the incident photoionization rate have been developed. They yield plasma temperature profiles in good
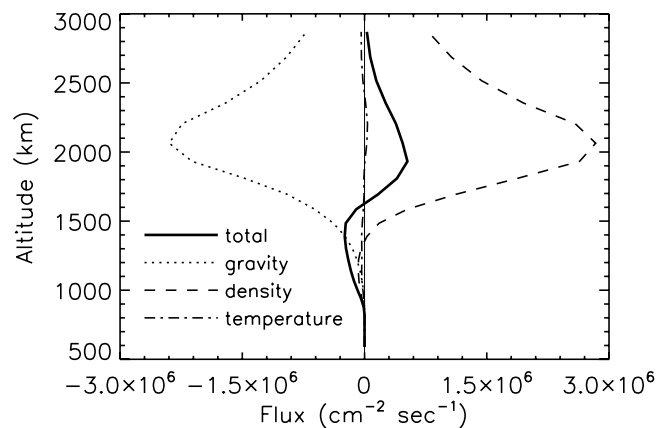

Figure 6. Modeled vertical flux for H^+ at 1700 LT for the identical conditions that lead to the plasma temperatures of Figure 3. The gravity, density, and temperature curves represent each of those processes' contributions to the net vertical flux.
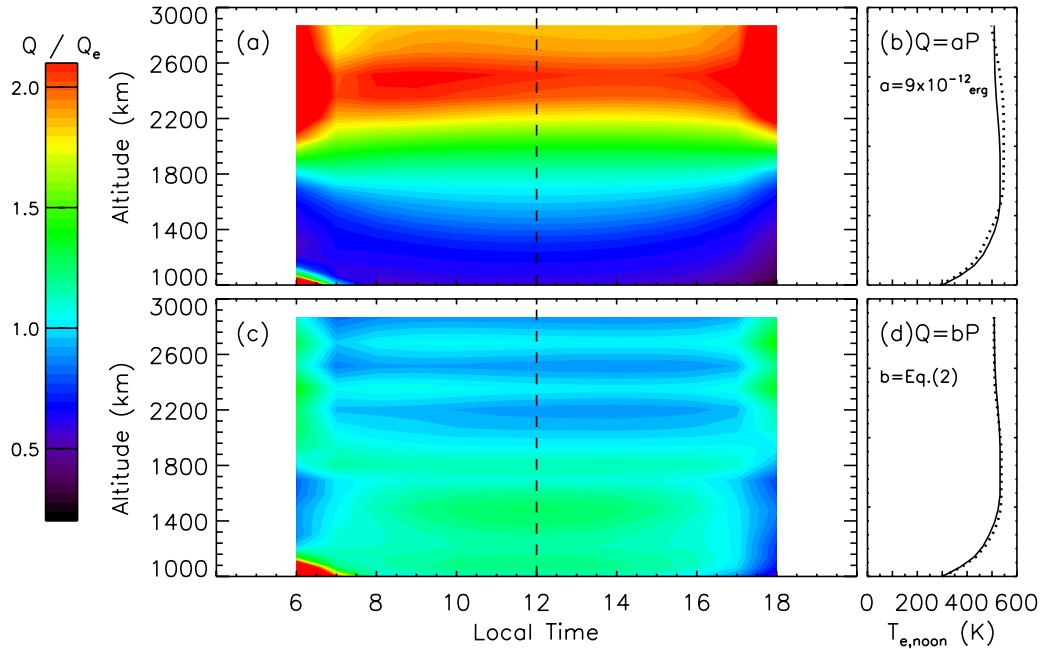
Figure 7. Figures 7a and 7c show diurnal variations of the ratio of two different parameterizations of the heating rate Q based on the photoionization rate P divided by the heating rate resulting from the full suprathermal transport calculation Q_e. Figures 7b and 7d show the resulting electron temperature profiles at local noon. (a) Ratio of heating rates for a simple parameterization where $Q = a P$ and $a = 9 \times 10^{-12}$ erg. (b) Electron temperatures resulting from the parameterization (dotted line) and the full transport calculation (solid line) at local noon. (c) Ratio of heating rates for a more complicated parameterization (see equation (2)). (d) Same as Figure 7b but the dotted line now shows the result for the parameterization given by equation (2).

agreement with calculations from a suprathermal electron transport code applied to photoelectrons and secondaries. While these parameterizations have been tested for only the conditions of the Voyager 2 Saturn flyby, their robustness across a wide range of solar zenith angles gives some confidence that they may be suitable for a wider range of conditions, and possibly for the hydrogen-rich upper atmospheres of other giant planets.

Appendix A: Suprathermal Electron Transport

[35] Assuming plane-parallel symmetry, the electron transport equation applied to photoelectrons can be written [*Oran and Strickland*, 1978; *Stamnes and Rees*, 1983]

$$
\mu \sin I \frac{\partial \Phi(z,E,\mu)}{\partial z} = -\sum_k n_k(z)\sigma_k^T(E)\Phi(z,E,\mu) + S(z,E,\mu)
$$
$$
+ n_e(z)\frac{\partial(L(E)\Phi(z,E,\mu))}{\partial E}
$$
$$
+ \sum_{k,\,pr} n_k(z)\sigma_k^T(E) \int_{-1}^{+1} d\mu'
$$
$$
\times \int_E^{E_{max}} dE' R_{k,\,pr}(E',\mu' \to E,\mu)\Phi(z,E',\mu')
$$

(A1)

where $\Phi(z, E, \mu)$ is the stationary electron flux (cm^{-2} s^{-1} eV^{-1} sr^{-1}); z is the altitude; E, E' are energies (eV) of scattered and incident electron angles; μ, μ' are cosines of scattered and incident electrons; $L(E)$ is the stopping cross section associated with the energy transfer from the

suprathermal to the thermal electrons [*Swartz et al.*, 1971; *Stamnes and Rees*, 1983]; $R_{k,pr}$ is the redistribution function describing the degradation from a higher energy state (E', μ') to the state (E, μ) for the neutral species k and process pr (e.g., ionization, excitation, elastic); $\sigma_k^T(E)$ is the total elastic and inelastic collision cross section for the neutral species k colliding with one electron at energy E; $n_k(z)$ is the density of the neutral species k; and $n_e(z)$ is the electron density.

[36] The second term on the right-hand side of equation (A1) is the sum of the primary photoelectron source resulting from solar EUV and soft X-ray ionization of the upper atmosphere and the internal source associated with the secondary electrons from electron impact ionization. The algorithm describing the solution to equation (A1) will not be presented here; rather the reader is directed to *Lummerzheim et al.* [1989]. The thermal electron heating rate is calculated following the formulation of *Schunk and Nagy* [1978].

Appendix B: Ion and Electron Energy Equations

[37] Rewriting equation (1) (from section 3) in terms of a change of temperature results in

$$
\frac{\Delta T}{\Delta t} = \frac{2}{3}\frac{1}{nk}[Q - L] - v\sin^2 I \frac{\partial T}{\partial z} - \frac{2}{3}T\sin^2 I \frac{\partial v}{\partial z}
$$
$$
+ \frac{2}{3}\frac{\sin^2 I}{nk}\frac{\partial}{\partial z}\left(\Gamma\frac{\partial T}{\partial z}\right)
$$

(B1)

The electron coefficient of thermal conductivity is given by an approximation derived by *Banks* [1966a] using mean free

path considerations that incorporated both Coulomb collisions and electron-neutral collisional damping. The resulting expression is

$$\Gamma_e = \frac{7.7 \times 10^5 T_e^{5/2}}{1 + 2.16 \times 10^4 \left(T_e^2/n_e\right) \sum\limits_n n_n \langle q_D \rangle_n} \text{eV cm}^{-1}\text{s}^{-1}\text{K}^{-1} \quad (B2)$$

where $\langle q_D \rangle_n$ is defined as the Maxwellian averaged electron momentum transfer cross section for collisions with the nth neutral species [*Schunk and Nagy*, 2008]. For Saturn's atmosphere, the relevant cross sections are [*Banks and Kockarts*, 1973; *Itikawa*, 1978]

$$\langle q_D \rangle_{He} = 5.6 \times 10^{-16} \text{cm}^2 \quad (B3)$$

$$\langle q_D \rangle_H = \left[54.7 - 7.45 \times 10^{-3} T_e\right] \times 10^{-16} \text{cm}^2 \quad (B4)$$

$$\langle q_D \rangle_{H2} = A \left[1 + BT_e^{0.5} - CT_e^{1.5} - DT_e^2\right] \text{cm}^2$$
$$A = 6.29 \times 10^{-16}$$
$$B = 3.23 \times 10^{-2} \quad (B5)$$
$$C = 1.16 \times 10^{-6}$$
$$D = 7.18 \times 10^{-9}.$$

[38] We make the assumption that there is a single ion species responsible for the majority of energy transfer. Near the topside this is a good approximation as H^+ is by far the dominant ion (Figure 4), and this is the region corresponding to the breakdown in thermal equilibrium at Jupiter [e.g., *Henry and McElroy*, 1969] (also confirmed for Saturn on the basis of this study). Therefore, the ion thermal conductivity coefficient is given by [*Banks and Kockarts*, 1973]

$$\Gamma_i = 4.6 \times 10^4 \rho_i^{-0.5} T_i^{2.5} \text{ eV cm}^{-1}\text{s}^{-1}\text{K}^{-1} \quad (B6)$$

where ρ is the mass of the ion species in *amu*. To gauge the accuracy of this assumption, we have compared calculations using (B6) against the generalized form of the ion thermal conductivity coefficient:

$$\Gamma_i = \sum \frac{n_j}{n_e} \frac{\Gamma_j'}{1 + \Gamma_j' \sum\limits_n (1/R_{jn})} \quad (B7)$$

where Γ_j' is the jth ion conductivity, as given in equation (B6), and the neutral damping factor R_{jn} is given by

$$R_{jn} = \frac{3}{4} \left(\frac{8kT_i}{\pi m_j}\right)^{1/2} \frac{n_j}{n_n} \frac{k}{\bar{Q}_{nj}} \quad (B8)$$

with the average momentum transfer cross section $\bar{Q}_{nj}$ being expressed as

$$\bar{Q}_{nj} = 13.3 \times 10^{-14} \left(\frac{\alpha_o}{\mu_{nj}}\right)^{1/2} \left(\frac{T_i}{\rho_j} + \frac{T_n}{\rho_n}\right)^{-1/2} \quad (B9)$$

In equation (B9), α_o is the neutral polarizability (H = 0.668; H_2 = 0.806; He = 0.205) and μ_{nj} the ion neutral reduced

mass. Calculations using both equations (B6) and (B7) do not reveal any significant difference in the resulting plasma temperatures; therefore, equation (B6) evaluated for H^+ stands as a good approximation at Saturn.

[39] The heating Q and loss L terms in equation (B1) result from external sources (suprathermal photoelectrons, auroral electrons and their secondaries, which heat the thermal electrons through Coulomb collisions and Joule heating, which preferentially heats the ions) and from collisions between electrons, ions and neutrals, where the warmer gas imparts energy to the cooler gas. The rate of energy exchange between ions and electrons is given by [*Schunk and Nagy*, 1978; *Banks and Kockarts*, 1973]

$$\frac{dU_{ie}}{dt} = \frac{4(2\pi m_e)^{0.5}}{m_i} n_e n_i \left(\zeta_i e^2\right)^2 \frac{k(T_e - T_i)}{(kT_e)^{1.5}} \ln \Lambda \quad (B10)$$

where ζ_i is the ion charge number, e the fundamental charge, and $\ln \Lambda$ the Coulomb logarithm. This expression can represent either a heat source or a loss for the electron population, depending on the values of T_e and T_i. The Coulomb logarithm is defined as [*Itikawa*, 1971]

$$\ln \Lambda = \ln \left\{ \frac{4kT_e}{r^2 \zeta_i e^2 f} \right\} - \frac{f^2 + d^2}{d^2} \ln \left[\frac{(d^2 + f^2)^{0.5}}{f} \right]$$
$$d^2 = \frac{4\pi n_i \zeta_i^2 e^2}{kT_i}$$
$$f^2 = \frac{4\pi n_e e^2}{kT_e} \quad (B11)$$

and $\ln r = 0.577 \equiv$ Euler's constant.

[40] The expression governing elastic electron-neutral interactions is [*Banks*, 1966b]

$$\frac{dU_{en}}{dt} = \left(\frac{128}{\pi}\right)^{0.5} n_e n_n (m_e kT_e)^{0.5} \frac{k(T_e - T_n)}{m_n} \langle q_D \rangle. \quad (B12)$$

(See also *Banks and Kockarts* [1973] and *Desloge* [1962].) The momentum transfer cross section $\langle q_D \rangle$ is given in equations (B3) − (B5). Rewriting equation (B12) with the constants inserted gives

$$H : \frac{dU_{en}}{dt} = 6.37 \times 10^{-16} n_e n_H T_e^{0.5} (T_e - T_n)$$
$$\cdot \left(1 - 1.35 \times 10^{-4} T_e\right) \text{eV cm}^{-3}\text{s}^{-1}$$

$$He : \frac{dU_{en}}{dt} = 1.63 \times 10^{-17} n_e n_{He} T_e^{0.5} (T_e - T_n) \text{eV cm}^{-3}\text{s}^{-1}$$

$$H_2 : \frac{dU_{en}}{dt} = 7.33 \times 10^{-17} n_e n_{H_2} T_e^{0.5} (T_e - T_n)$$
$$\cdot \left(1 + BT_e^{0.5} - CT_e^{1.5} - DT_e^2\right) \text{eV cm}^{-3}\text{s}^{-1}.$$

[41] In addition, electrons interact with molecular hydrogen via rotational and vibrational excitation of H_2. The high relative concentration of H_2 in the atmosphere and the large cross sections for vibrational and rotational excitation of H_2 by electrons make these interactions the dominant electron-neutral energy exchange processes in Saturn's ionosphere. The rates of rotational and vibrational electron-H_2 energy

exchange are [*Waite and Cravens*, 1981; *Schunk and Nagy*, 2008]

$$\frac{dU}{dt}_{rot} = 2.278 \times 10^{-11}$$
$$\cdot \left\{ \exp\left[2.093 \times 10^{-4} (T_e - T_n)^{1.078} - 1 \right] \right\} eV \ cm^{-3} s^{-1}$$
(B13)

and

$$\frac{dU}{dt}_{vib} = 1.17 \times 10^{-6} k n_e n_{H_2} \exp\left[\frac{-5253.7}{T_e - T_n} \right] eV \ cm^{-3} s^{-1} \quad (B14)$$

respectively.

[42] Finally, ions can collide with neutrals, resulting in elastic and resonant charge exchange reactions. The rate of the resonant charge exchange reaction for a Maxwellian distribution of H^+ ions and H atoms may be expressed [*Banks*, 1966b]

$$\frac{dU_{in}}{dt} = 1.4 \times 10^{-14} n_H n_{H^+} (T_i + T_n)^{0.5} (T_i - T_n) eV \ cm^{-3} s^{-1}.$$
(B15)

As H^+ is the dominant ion, and H an important neutral constituent (especially at high altitudes), equation (B15) represents the dominant ion-neutral energy exchange process for Saturn's ionosphere.

[43] In order to solve for plasma temperatures in Saturn's ionosphere, first the standard model is run to steady state with the assumption of $T_e = T_i = T_n$. At this point, equation (B1) and the various rates of ion-electron, ion-neutral and electron-neutral energy exchange are iterated in time, along with the ion and electron density calculations described above. The lower boundary condition is $T_e = T_i = T_n$, although in practice this does not need to be enforced as there is no significant heating at that altitude (Figure 3). At the upper boundary, the temperature gradients are held constant, and assigned the value of the grid point immediately below the top.

References

Achilleos, N., S. Miller, J. Tennyson, A. D. Aylward, I. Mueller-Wodarg, and D. Rees (1998), JIM: A time-dependent, three-dimensional model of Jupiter's thermosphere and ionosphere, *J. Geophys. Res.*, *103*, 20089–20112, doi:10.1029/98JE00947.

Atreya, S. K., J. H. Waite, T. M. Donahue, A. F. Nagy, and J. C. McConnell (1984), Theory, measurements and models of the upper atmosphere and ionosphere of Saturn, in *Saturn*, edited by E. Gehrels, pp. 239–277, Univ. of Ariz. Press, Tucson.

Banks, P. (1966a), Collision frequencies and energy transfer electrons, *Planet. Space Sci.*, *14*, 1085–1103, doi:10.1016/0032-0633(66)90024-9.

Banks, P. (1966b), Collision frequencies and energy transfer ions, *Planet. Space Sci.*, *14*, 1105–1122, doi:10.1016/0032-0633(66)90025-0.

Banks, P. (1967), The temperature coupling of ions in the ionosphere, *Planet. Space Sci.*, *15*, 77–93, doi:10.1016/0032-0633(67)90068-2.

Banks, P. M., and G. Kockarts (1973), *Aeronomy*, Elsevier, New York.

Bourdeau, R. E. (1963), Ionospheric research from space vehicles, *Space Sci. Rev.*, *1*, 683–728, doi:10.1007/BF00212448.

Chapman, S., and T. G. Cowling (1970), *The Mathematical Theory of Non-uniform Gases: An Account of the Kinetic Theory of Viscosity, Thermal Conduction and Diffusion in Gases*, Cambridge Univ. Press, Cambridge, U. K.

Cicerone, R. J., and S. A. Bowhill (1971), Photoelectron fluxes measured at Millstone Hill, *Radio Sci.*, *6*, 957–966, doi:10.1029/RS006i011p00957.

Cicerone, R. J., W. E. Swartz, R. S. Stolarski, A. F. Nagy, and J. S. Nisbet (1973), Thermalization and transport of photoelectrons: A comparison of theoretical approaches, *J. Geophys. Res.*, *78*, 6709–6728, doi:10.1029/JA078i028p06709.

Davis, L., Jr., and E. J. Smith (1990), A model of Saturn's magnetic field based on all available data, *J. Geophys. Res.*, *95*, 15,257–15,261, doi:10.1029/JA095iA09p15257.

Desloge, E. A. (1962), Coefficients of diffusion, viscosity, and thermal conductivity of a gas, *Am. J. Phys.*, *30*, 911–920, doi:10.1119/1.1941848.

Fuller-Rowell, T. J., D. Rees, S. Quegan, R. J. Moffett, M. V. Codrescu, and G. H. Millward (1996), A coupled thermosphere-ionosphere model (CTIM), in *STEP: Handbook of Ionospheric Models*, edited by R. W. Schunk, pp. 217–238, Sci. Comm. on Sol. Terr. Phys., Utah State Univ., Logan.

Galand, M., J. Lilensten, D. Toublanc, and S. Maurice (1999), The ionosphere of Titan: Ideal diurnal and nocturnal cases, *Icarus*, *140*, 92–105, doi:10.1006/icar.1999.6113.

Galand, M., R. V. Yelle, A. J. Coates, H. Backes, and J.-E. Wahlund (2006), Electron temperature of Titan's sunlit ionosphere, *Geophys. Res. Lett.*, *33*, L21101, doi:10.1029/2006GL027488.

Glocer, A., T. I. Gombosi, G. Toth, K. C. Hansen, A. J. Ridley, and A. Nagy (2007), Polar wind outflow model: Saturn results, *J. Geophys. Res.*, *112*, A01304, doi:10.1029/2006JA011755.

Goertz, C. K. (1973), Jupiter's ionosphere and magnetosphere, *Planet. Space Sci.*, *21*, 1389–1398, doi:10.1016/0032-0633(73)90231-6.

Henry, R. J. W., and M. B. McElroy (1969), The absorption of extreme ultraviolet solar radiation by Jupiter's upper atmosphere, *J. Atmos. Sci.*, *26*, 912–917, doi:10.1175/1520-0469(1969)026<0912:TAOEUS>2.0.CO;2.

Hubbard, W. B., et al. (1997), Structure of Saturn's mesosphere from the 28 Sgr occultations, *Icarus*, *130*, 404–425, doi:10.1006/icar.1997.5839.

Itikawa, Y. (1971), Effective collision frequency of electrons in atmospheric gases, *Planet. Space Sci.*, *19*, 993–1007.

Itikawa, Y. (1978), Electron scattering by polar molecules, *Phys. Rep.*, *46*, 117–164, doi:10.1016/0370-1573(78)90164-3.

Lei, J., R. G. Roble, W. Wang, B. A. Emery, and S. R. Zhang (2007), Electron temperature climatology at Millstone Hill and Arecibo, *J. Geophys. Res.*, *112*, A02302, doi:10.1029/2006JA012041.

Lilensten, J., W. Kofman, J. Wisemberg, E. S. Oran, and C. R. Devore (1989), Ionization efficiency due to primary and secondary photoelectrons—A numerical model, *Ann. Geophys.*, *7*, 83–90.

Lindal, G. F., D. N. Sweetnam, and V. R. Eshleman (1985), The atmosphere of Saturn—An analysis of the Voyager radio occultation measurements, *Astron. J.*, *90*, 1136–1146, doi:10.1086/113820.

Lummerzheim, D., and J. Lilensten (1994), Electron transport and energy degradation in the ionosphere: Evaluation of the numerical solution. Comparison with laboratory experiments and auroral observations, *Ann. Geophys.*, *12*, 1039–1051.

Lummerzheim, D., M. H. Rees, and H. R. Anderson (1989), Angular dependent transport of auroral electrons in the upper atmosphere, *Planet. Space Sci.*, *37*, 109–129, doi:10.1016/0032-0633(89)90074-3.

Majeed, T., and J. C. McConnell (1991), The upper ionospheres of Jupiter and Saturn, *Planet. Space Sci.*, *39*, 1715–1732, doi:10.1016/0032-0633(91)90031-5.

Matcheva, K. I., and D. F. Strobel (1999), Heating of Jupiter's thermosphere by dissipation of gravity waves due to molecular viscosity and heat conduction, *Icarus*, *140*, 328–340, doi:10.1006/icar.1999.6151.

Miller, S., et al. (2000), The role of H_3^+ in planetary atmospheres, *Philos. Trans. R. Soc. London, Ser. A*, *358*, 2485–2501, doi:10.1098/rsta.2000.0662.

Millward, G. H., R. J. Moffett, W. Quegan, and T. J. Fuller-Rowell (1996), A coupled thermospheric-ionospheric-plasmasphere model (CTIP), in *STEP: Handbook of Ionospheric Models*, edited by R. W. Schunk, pp. 239–279, Sci. Comm. on Sol. Terr. Phys., Utah State Univ., Logan.

Moore, L., and M. Mendillo (2005), Ionospheric contribution to Saturn's inner plasmasphere, *J. Geophys. Res.*, *110*, A05310, doi:10.1029/2004JA010889.

Moore, L., and M. Mendillo (2007), Are depletions in Saturn's ionosphere caused by explosive surges of water from Enceladus?, *Geophys. Res. Lett.*, *34*, L12202, doi:10.1029/2007GL029381.

Moore, L. E., M. Mendillo, I. C. F. Mueller-Wodarg, and D. L. Murr (2004), Modeling of global variations and ring shadowing in Saturn's ionosphere, *Icarus*, *172*, 503–520, doi:10.1016/j.icarus.2004.07.007.

Moore, L., A. F. Nagy, A. J. Kliore, I. Mueller-Wodarg, J. D. Richardson, and M. Mendillo (2006), Cassini radio occultations of Saturn's ionosphere: Model comparisons using a constant water flux, *Geophys. Res. Lett.*, *33*, L22202, doi:10.1029/2006GL027375.

Moses, J. I., and S. F. Bass (2000), The effects of external material on the chemistry and structure of Saturn's ionosphere, *J. Geophys. Res.*, *105*, 7013–7052, doi:10.1029/1999JE001172.

Moses, J. I., B. Bezard, E. Lellouch, G. R. Gladstone, H. Feuchtgruber, and M. Allen (2000), Photochemistry of Saturn's atmosphere, I, Hydrocarbon chemistry and comparisons with ISO observations, *Icarus*, *143*, 244–298, doi:10.1006/icar.1999.6270.

Mueller-Wodarg, I. C. F., M. Mendillo, R. V. Yelle, and A. D. Aylward (2006), A global circulation model of Saturn's thermosphere, *Icarus*, *180*, 147–160, doi:10.1016/j.icarus.2005.09.002.

Nagy, A. F., and P. M. Banks (1970), Photoelectron fluxes in the ionosphere, *J. Geophys. Res.*, *75*, 6260–6270, doi:10.1029/JA075i031p06260.

Nagy, A. F., W. L. Chameides, R. H. Chen, and S. K. Atreya (1976), Electron temperatures in the Jovian ionosphere, *J. Geophys. Res.*, *81*, 5567–5569, doi:10.1029/JA081i031p05567.

Nagy, A. F., A. R. Barakat, and R. W. Schunk (1986), Is Jupiter's ionosphere a significant plasma source for its magnetosphere?, *J. Geophys. Res.*, *91*, 351–354, doi:10.1029/JA091iA01p00351.

Nagy, A. F., et al. (2006), First results from the ionospheric radio occultations of Saturn by the Cassini spacecraft, *J. Geophys. Res.*, *111*, A06310, doi:10.1029/2005JA011519.

Nilsson, H., S. Kirkwood, J. Lilensten, and M. Galand (1996), Enhanced incoherent scatter plasma lines, *Ann. Geophys.*, *14*, 1462–1472, doi:10.1007/s005850050407.

Nisbet, J. S. (1968), Photoelectron escape from the ionosphere, *J. Atmos. Terr. Phys.*, *30*, 1257–1278, doi:10.1016/S0021-9169(68)91090-8.

Oran, E. S., and D. J. Strickland (1978), Photoelectron flux in the Earth's ionosphere, *Planet. Space Sci.*, *26*, 1161–1177, doi:10.1016/0032-0633(78)90056-9.

Porco, C. C., et al. (2006), Cassini observes the active South Pole of Enceladus, *Science*, *311*, 1393–1401, doi:10.1126/science.1123013.

Prasad, S. S., and L. A. Capone (1971), The Jovian ionosphere: Composition and temperatures, *Icarus*, *15*, 45–55, doi:10.1016/0019-1035(71)90032-7.

Richards, P. G., and G. V. Khazanov (1997), On the thermal electron energy balance in the ionosphere in January 1993 and June 1990, *J. Geophys. Res.*, *102*, 7369–7378, doi:10.1029/96JA03104.

Richards, P. G., J. A. Fennelly, and D. G. Torr (1994), EUVAC: A solar EUV flux model for aeronomic calculations, *J. Geophys. Res.*, *99*, 8981–8992, (Correction: J. Geophys. Res., 99, 13,283–13,284), doi:10.1029/94JA00518.

Rishbeth, H., and O. K. Garriott (1969), *Introduction to Ionospheric Physics*, Academic, San Diego, Calif.

Roble, R., and E. Ridley (1994), A thermosphere-ionosphere-mesosphere-electrodynamics general circulation model (time-GCM): Equinox solar cycle minimum simulations (30–500 km), *Geophys. Res. Lett.*, *21*, 417–420, doi:10.1029/93GL03391.

Roble, R. G., E. C. Ridley, and R. E. Dickinson (1987), On the global mean structure of the thermosphere, *J. Geophys. Res.*, *92*, 8745–8758, doi:10.1029/JA092iA08p08745.

Schunk, R. W., and A. F. Nagy (1978), Electron temperatures in the F region of the ionosphere: Theory and observations, *Rev. Geophys.*, *16*, 355–399, doi:10.1029/RG016i003p00355.

Schunk, R. W., and A. F. Nagy (2008), *Ionospheres*, 2nd ed., Cambridge Univ. Press, Cambridge, U. K., in press.

Smith, G. R., D. E. Shemansky, J. B. Holberg, A. L. Broadfoot, B. R. Sandel, and J. C. McConnell (1983), Saturn's upper atmosphere from the Voyager 2 EUV solar and stellar occultations, *J. Geophys. Res.*, *88*, 8667–8678, doi:10.1029/JA088iA11p08667.

Stamnes, K., and M. H. Rees (1983), Inelastic scattering effects on photoelectron spectra and ionospheric electron temperature, *J. Geophys. Res.*, *88*, 6301–6309, doi:10.1029/JA088iA08p06301.

Strickland, D. J., D. L. Book, T. P. Coffey, and J. A. Fedder (1976), Transport equation techniques for the deposition of auroral electrons, *J. Geophys. Res.*, *81*, 2755–2764, doi:10.1029/JA081i016p02755.

Swartz, W. E., and J. S. Nisbet (1972), Revised calculations of F region ambient electron heating by photoelectrons, *J. Geophys. Res.*, *77*, 6259–6261, doi:10.1029/JA077i031p06259.

Swartz, W. E., J. S. Nisbet, and A. E. S. Green (1971), Analytic expression for the energy transfer rate from photoelectrons to thermal electrons, *J. Geophys. Res.*, *76*, 8425–8426, doi:10.1029/JA076i034p08425.

Swartz, W. E., R. W. Reed, and T. R. McDonough (1975), Photoelectron escape from the ionosphere of Jupiter, *J. Geophys. Res.*, *80*, 495–501, doi:10.1029/JA080i004p00495.

Tyler, G. L., V. R. Eshleman, J. D. Anderson, G. S. Levy, G. F. Lindal, G. E. Wood, and T. A. Croft (1982), Radio science with Voyager 2 at Saturn—Atmosphere and ionosphere and the masses of Mimas, Tethys, and Iapetus, *Science*, *215*, 553–558, doi:10.1126/science.215.4532.553.

Waite, J. H. (1981), The ionosphere of Saturn, thesis, Univ. of Mich., Ann Arbor.

Waite, J. H., Jr., and T. E. Cravens (1981), Vibrational and rotational cooling of electrons by molecular hydrogen, *Planet. Space Sci.*, *29*, 1333–1338, doi:10.1016/0032-0633(81)90099-4.

Waite, J. H., et al. (2006), Cassini Ion and Neutral Mass Spectrometer: Enceladus plume composition and structure, *Science*, *311*, 1419–1422, doi:10.1126/science.1121290.

Yelle, R. V., and S. Miller (2004), Jupiter's thermosphere and ionosphere, in *Jupiter: The Planet, Satellites, and Magnetosphere*, edited by F. Bagenal et al., pp. 185–218, Cambridge Univ. Press, New York.

————————————

M. Galand and I. Mueller-Wodarg, Space and Atmospheric Physics Group, Department of Physics, Imperial College London, Prince Consort Road, London SW7 2BW, UK.

M. Mendillo and L. Moore, Center for Space Physics, Boston University, 725 Commonwealth Avenue, Boston, MA 02215, USA. (moore@bu.edu)

R. Yelle, Lunar and Planetary Laboratory, University of Arizona, 1629 East University Boulevard, Tucson, AZ 85721, USA.